JOC The Journal of Organic Chemistry

Article

pubs.acs.org/joc

Nature of Electrogenerated Intermediates in Nitro-Substituted Nor-β-lapachones: The Structure of Radical Species during Successive Electron Transfer in Multiredox Centers

Georgina Armendáriz-Vidales,[†] Lindsay S. Hernández-Muñoz,[‡] Felipe J. González,[‡] Antonio A. de Souza,[∥] Fabiane C. de Abreu,[∥] Guilherme A. M. Jardim,[§] Eufrânio N. da Silva, Jr.,[§] Marilia O. F. Goulart,*[,∥] and Carlos Frontana*[,†]

[†]Centro de Investigación y Desarrollo Tecnológico en Electroquímica, S.C., Parque Tecnológico Querétaro Sanfandila, 76703 Pedro Escobedo, Querétaro Mexico

[‡]Departamento de Química, Centro de Investigación y de Estudios Avanzados del I.P.N., Apartado Postal 14-740, 07360 México, D.F., Mexico

[∥]Instituto de Química e Biotecnologia, Universidade Federal de Alagoas, Tabuleiro do Martins, Maceió, Alagoas 57072-970, Brazil

[§]Laboratório de Química Sintética e Heterocíclica, Instituto de Ciências Exatas, Departamento de Química, Universidade Federal de Minas Gerais, 31270-901, Belo Horizonte, MG Brazil

Supporting Information

ABSTRACT: Electrochemical, spectroelectrochemical, and theoretical studies of the reduction reactions in nor-β-lapachone derivatives including a nitro redox center showed that reduction of the compounds involves the formation of several radical intermediates, including a biradical dianion resultant from the separate reduction of the quinone and nitro groups in the molecules. Theoretical descriptions of the corresponding Fukui functions $f^{+}_{\alpha\alpha}$ and $f^{+}_{\beta\beta}(\mathbf{r})$ and LUMO densities considering finite differences and frozen core approximations for describing the changes in electron and spin densities of the system allowed us to confirm these results. A description of the potential relationship with the obtained results and biological activity selectivity indexes suggests that both the formation of stable biradical dianion species and the stability of the semiquinone intermediates during further reduction are determining factors in the description of their biological activity.

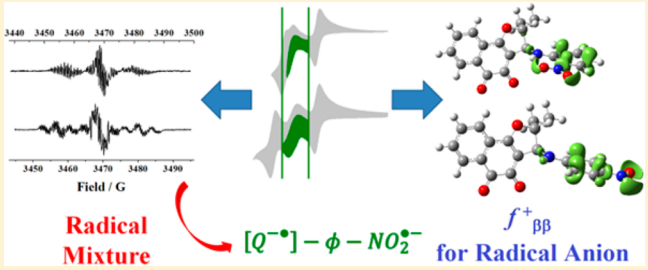

1. INTRODUCTION

Interaction between electroactive groups is determinant in the reactivity of molecules bearing multiple redox centers, as it has already been described for transition-metal units, polymers,[1−3] polyorganic compounds,[4−6] biological macromolecules,[6] among others. This interaction is evidenced by the difference in redox potential values for each site, which depends on the extent of solvation and structural changes, along with the formation of ion pairs and the degree of delocalization of the charge in the multicharged structure.[6]

Electrochemical studies are typically employed for analyzing the mutual influence of the redox groups. For this purpose, several factors should be considered, such as position, number, size, and shape of the involved voltammetric peaks. For example, the removal of the first electron from a fluorene-containing oligomer shifted to a less positive potential as the number of fluorene unites increases.[7] Also, for mixed valence complexes of ruthenium, the difference in potential values between redox centers suggested that the degree of delocalization is dependent on the electronic communication between them.[8] Telo and co-workers, by means of spectroelectrochemical experiments, proved that reduction of dinitrodibenzodioxin radical anions is followed by intramolecular electron transfer, evidencing the communication between each nitro function.[9] Changes in the intermolecular interactions (e.g., hydrogen-bond ability, changes in dipolar moment, etc.) are clearly capable of affecting the structures, reactivities, biological activities, equilibria, reaction rate constants, and other aspects that are of central interest to chemistry and biology.[10]

Multielectronic electron transfer can also be of great importance in biological processes, in which stable reduced intermediates from organic compounds are involved.[11−13] For example, nor-β-lapachone derivatives (Figure 1) bearing two electroactive groups (quinone and nitroaromatic) have been synthesized and studied recently.[14] These compounds showed significant cytotoxicity against tumoral cell lines[15] as well as

Received: April 7, 2014
Published: May 1, 2014

   dx.doi.org/10.1021/jo500787q | J. Org. Chem. 2014, 79, 5201−5208

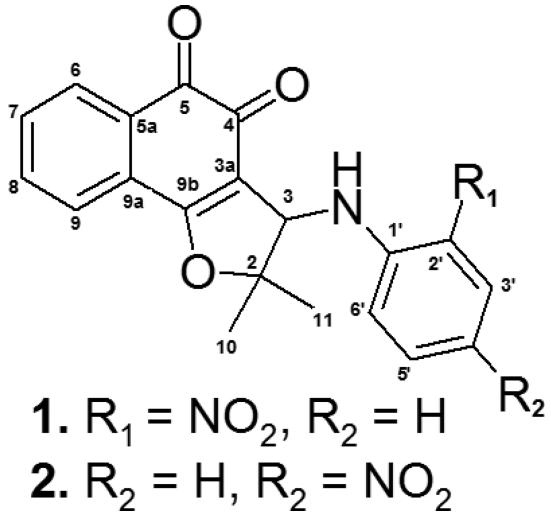

Figure 1. Nor-β-lapachone arylamino-substituted compounds.

high activity as trypanocidal agents[15,16] (Table 1), compared with the reference compounds (doxorubicin and benznidazole).

The selectivity of nor-β-lapachone derivatives (an *o*-quinone) is high toward cancer cells. Interestingly, selectivity seems to be dependent on the presence of a nitro group: *ortho* (**1**) and *para* (**2**) nitro-substituted derivatives showed higher selectivity indexes (Table 1) than doxorubicin.[18] Concerning trypanocidal activity, **1** is significantly active, compared with benznidazole, differently from compound **2** that is inactive.[16,17] These results suggest that for this last biological mechanism of action the position of the nitro function becomes more relevant and is independent of the presence of the quinone moiety. Consequently, molecular interactions between both electroactive groups modulate the specific mechanism of biological activity for each functional group.

Previous electrochemical and spectroelectrochemical analyses of nor-β-lapachone derivatives evidenced the presence of radical intermediates,[19] which are related to the specific biological mechanisms of action activity mentioned earlier. Therefore, a molecular-based description on the chemical nature of the electrogenerated intermediates and their stability is desirable in order to improve our knowledge in pharmacological aspects.

Reactivity indexes regarding electron-transfer processes obtained from electronic structure calculations have demonstrated their utility in identifying the sites of the molecule prone to electron acceptance.[20−24] From density functional theory, a particular index, named the Fukui function ($f^{\pm}(r)$),[25] is defined as

$$f^{\pm}(r) = \left(\frac{\partial \rho(r)}{\partial N}\right)_{\nu(r)} \quad (1)$$

This function represents the change in electron density ($\rho(r)$) when the number of electrons (N) in the system changes at a constant external potential ($\nu(r)$). The corresponding sign is related to cases where an electron is gained (positive), or lost (negative), from the structure. In the case of an electron transfer, it should be noticed that, besides the change in the number of electrons in the system, the difference in α, and β, electron populations is also affected; this effect leads also to changes in the spin of the system, resulting in different situations, based on the changes in spin between the reactant and product molecules.[26] Even though the Fukui function is a widely employed descriptor, it has been scarcely used for systems having multiple redox centers,[27,28] and for these kind of compounds it would provide a description on the sites associated with each successive electron-transfer step.

In this work, an electrochemical, ESR-spectroelectrochemical, and theoretical analysis of *o*- and *p*-nitro nor-β-lapachone compounds (**1** and **2**, respectively) (Figure 1) is presented. The use of spin dependent local reactivity descriptors based on the Fukui functions is highlighted in order to provide information on the changes of both charge and spin states, which have relevant implications for the understanding of the reduction mechanisms of these compounds.

2. RESULTS AND DISCUSSION

2.1. Electrochemical Characterization of the studied compounds. Cyclic voltammograms for 1×10^{-3} mol L^{-1} solutions of **1** and **2** were obtained in the potential region between the open circuit potential, −0.26 V and −2.7 V vs Fc/Fc^{+} (Figure 2).

Both compounds present three main reversible one-electron signals (Ic/Ia, IIc/IIa, and IIIc/IIIa), followed by an irreversible reduction peak IVc (Figure 2). It should be noted that the difference in potential values between reversible systems IIc/IIa and IIIc/IIa is larger in compound **2** than in **1**, and in this last compound, the system IIc/IIa is observed as a voltammetric shoulder. Half-wave potential values ($E_{1/2}$) for the correspond-

Table 1. Reported Cytotoxic (μM) and Trypanocidal Activities Concerning Compounds 1 and 2, and Their Precursors, Together with Selectivity Index (SI), Where SI = Cytotoxicity (μM) against Peripheral Blood Mononuclear Cells (PBMC)/ Cytotoxicity (μM) against Cancer Cell Lines[a]

compd	HL-60	MDAMB- 435	SF-295	HCT- 8	PC-3	PBMC	TA vs TC[b]
1[16,18]	1.18	0.74	1.59	1.78	0.66	12.02	55.6 ± 4.6
SI	10.18	20.48	5.76	8.07	>18		
2[17,18]	0.96	0.19	0.76	0.82	0.51	5.02	857.3 ± 96.4
SI	5.23	26.42	6.12	6.60	9.84		
nor-β-lapachone[18]	1.75	0.31	1.36	1.58	1.98	>21.9	>4800
SI	>12	>20	>16	>14	>11		
doxorubicin	0.03	0.88	0.06	0.41		0.42	
SI	14	0.48	7	1.02			
benznidazole[16]							103.6 ± 0.6

[a]HL-60: leukemia, IM; MDA-MB-435: melanoma, IM; SF-295: central nervous system, IM; HCT-8: colon, IM; PC-3: prostate; PBMC: peripheral blood mononuclear cells, TA: Trypanocidal activity against *T. cruzi*. [b]IC_{50}/24 h (μM).

dx.doi.org/10.1021/jo500787q | J. Org. Chem. 2014, 79, 5201−5208

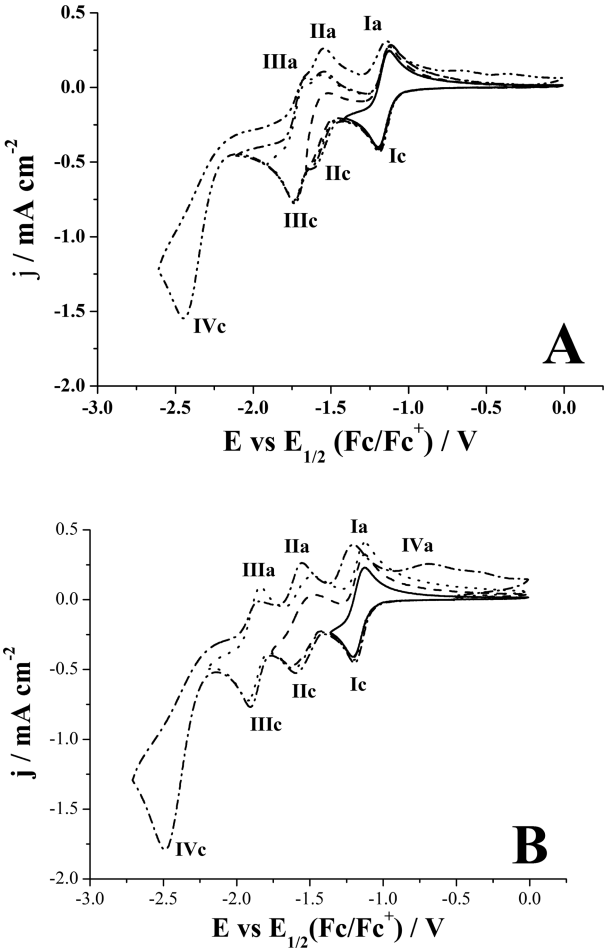

Figure 2. Cyclic voltammograms of 1×10^{-3} mol L^{-1} solutions of (A) **1** and (B) **2** in CH_3CN/0.1 mol L^{-1} *n*-Bu_4NPF_6. Voltammograms at different inversion potential conditions are shown [scan rate (ν) = 100 mV s^{-1}; glassy carbon (GC) working electrode, area = 0.07 cm^2].

ing peak couples, along with cathodic peak potential of signal IV are shown in Table 2.

Table 2. Potential Values for Compounds 1 and 2 vs $E_{1/2}$ (Fc/Fc^+)/V

	$E_{1/2}$			
compd	I	II	III	Ep_{IVc}
1	−1.20	−1.61	−1.73	−2.45
2	−1.20	−1.60	−1.90	−2.50

Due to the presence of both quinone and nitroaromatic moieties in nor-β-derivatives, it is not possible to directly assign the observed signals to a given reaction in the third process, since two possible electrogenerated radicals can be formed from the original structure (represented by [Q]-ϕ-NO_2): [$Q^{\bullet-}$]-ϕ-NO_2 or [Q]-ϕ-$NO_2^{\bullet-}$. In order to discriminate between both possibilities, ESR-electrochemical experiments were carried out. In the case of compound **2**, due to the large separation of the waves, this would be of fundamental importance.

Upon reduction of 1×10^{-3} mol L^{-1} solutions of both compounds, at a constant potential between peaks Ic and IIc (Figure 2), ESR patterns for stable radicals were detected (Figure 3).

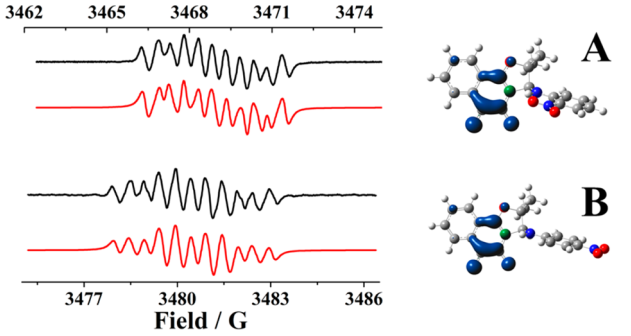

Figure 3. ESR spectra obtained upon reduction of a 1×10^{-3} mol L^{-1} solution of (A) **1** and (B) **2** in CH_3CN/0.1 mol L^{-1} *n*-Bu_4NPF_6 at E = −1.35 V vs $E_{1/2}$ (Fc/Fc^+). Spectra in black represent experimental data while those in red indicate simulated hyperfine structures. Isosurfaces of the spin density of the anion radical structures at 0.004 $Å^{-3}$ are also represented.

ESR spectra consists of hyperfine splitting related to the interaction between the nuclear spin of H atoms with the unpaired electron of the corresponding radical anion; the assignment of the experimental hyperfine coupling constants (HFCC) was performed when comparing experimental values to theoretical HFCC data acquired from the electronic structure calculations (Table 3), leading to the estimation of 5 HFCC values, which are in accordance with the formation of a semiquinone-type radical. Spin density in this semiquinone extends toward the substituent at position C-3, as validated from theoretical calculations (Figure 3).

Upon continuing the potential scan toward more negative values than −1.5 V vs Fc/Fc^+, the formation of a secondary signal from a new radical species (Figure 4) was observed in both compounds. This last signal was stable (Figure 5) during application of the potential step and was followed by a slow consumption of the former radical (Figure 3).

At potential values more negative than peak IIIc (−1.8 vs $E_{1/2}$ (Fc/Fc^+), Figure 2, the secondary signal prevailed while the one related to the semiquinone disappeared. The resulting spectra are presented in Figure 5.

The second radical anion observed is consistent with coupling with the N nuclei from the $-NO_2$ group at C-2′ or C-4′, and the remaining signals are associated with coupling with the H atoms in the structure (Table 3). It is worth mentioning that in the case of the *para* compound **2**, two additional sets of HFCC values were considered: the first one involves interaction between the spin and the hydrogen atoms at positions C-3 and of the NH group. Also, an extra triplet structure from interaction with an atom of S = 1 was considered in the simulation, suggesting that for this radical species, coupling with the N atom of the NH group is possible, differently for the corresponding radical anion in compound **1**. During the analysis of the calculated spin densities between both compounds, HFCC for the N atom for compound **1** is significantly lower (0.04 G), compared with the one obtained for the same N atom in compound **2** (0.25 G, Table 2), validating the proposed coupling. The observed diminishment of the signal from the electrogenerated semiquinone (Figure 5) indicates that the semiquinone electrogenerated at peak Ic is being consumed at peak IIIc to generate the corresponding dianion. The remaining radical from the nitro group is consumed at peak IVc (Figure 2).

dx.doi.org/10.1021/jo500787q | J. Org. Chem. 2014, 79, 5201−5208

Table 3. Hyperfine Coupling Constants and Linewidths for the Electrogenerated Radical Anion Structures for Compounds 1 and 2[a]

radical structures	a_1 (G)	a_2 (G)	a_3 (G)	a_4 (G)	a_5 (G)	Γ (G)
first radical anion (**1**)[b]	1.43 [1.92] (H-3)	1.15 [1.59] (H-8)	1.01 [1.02] (H-6)	0.89 [0.86] (H-7)	0.6 [0.18] (H-9)	0.20
second radical anion (**1**)[c]	11.90 [6.11] (N-2′)	3.33 [2.98, 2.70] (H-3′, H-5′)	1.59 [1.54] (H-4′)	1.10 [1.01] (H-6′)	0.68 [0.42] (NH)	0.18
first radical anion (**2**)[b]	1.54 [1.95] (H-3)	1.47 [1.60] (H-8)	0.93 [0.87] (H-6)	0.59 [0.52] (H-7)	0.45 [0.19] (H-9)	0.20
second radical anion (**2**)[c]	11.78 [6.13] (N-4′)	3.71 [2.83, 2.56] (H-3′, H-5′)	1.15 [1.57, 1.62] (H-2′, H-6′)	0.44 [0.02, 0.71] (NH, H-3)	0.38 [0.25] (N-3)	0.20

[a]Assignments for each hyperfine coupling constant with the corresponding hydrogen atom are indicated for each signal (see Figure 1 for numbering). Numbers in brackets corresponds to calculated HFCC from BHandHLYP/6-311G++(d,p) considering the solvent effect by the Cramer and Truhlar model. [b]Radical obtained upon reduction at $E = -1.35$ V vs Fc/Fc$^+$. [c]Radical obtained upon reduction at $E = -1.80$ V vs Fc/Fc$^+$. NA: not applicable.

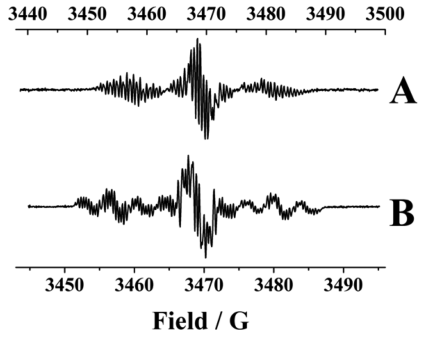

Figure 4. ESR spectra obtained upon reduction of a 1×10^{-3} mol L^{-1} solution of (A) **1** and (B) **2** in CH_3CN/0.1 mol L^{-1} n-Bu_4NPF_6 at E = −1.60 V (A) and −1.75 V (B) vs $E_{1/2}$ (Fc/Fc$^+$).

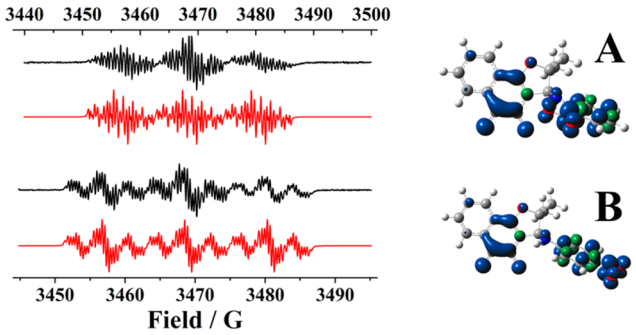

Figure 5. ESR spectra obtained upon reduction of a 1×10^{-3} mol L^{-1} solution of (A) **1** and (B) **2** in CH_3CN/0.1 mol L^{-1} n-Bu_4NPF_6 at $E = -1.8$ V vs $E_{1/2}$ (Fc/Fc$^+$). Spectra in black represent experimental data while those in red indicate simulated hyperfine structures. Isosurfaces of the spin density of anion radical structures at 0.004 Å^{-3} are also represented.

The description of the reduction processes can be explained using the following chemical equations. For peak Ic, the reaction occurring is

$$[Q]\text{-}\phi\text{-}NO_2 + e^- \rightleftarrows [Q^{\bullet -}]\text{-}\phi\text{-}NO_2 \quad (2)$$

This last product is being reduced at peak IIc for both compounds to form the corresponding biradical dianion species $[Q^{\bullet -}]$-ϕ-$NO^{\bullet -}{}_2$ following the reaction

$$[Q^{\bullet -}]\text{-}\phi\text{-}NO_2 + e^- \rightleftarrows [Q^{\bullet -}]\text{-}\phi\text{-}NO_2{}^{\bullet -} \quad (3)$$

During voltammetric peak IIIc, the semiquinone is being consumed to form the quinone dianion, keeping the nitro radical anion unaltered:

$$[Q^{\bullet}]\text{-}\phi\text{-}NO_2{}^{\bullet -} + e^- \rightleftarrows [Q^{2-}]\text{-}\phi\text{-}NO_2{}^{\bullet -} \quad (4)$$

The stability of this latter intermediate ($[Q^{2-}]$-ϕ-$NO_2{}^{\bullet -}$) depends on the relative position of the nitro group and can be quantitatively analyzed considering the differences for $E_{1/2}$ values between systems Ic/Ia and IIIc/IIIa: the corresponding values are 0.53 V for **1**, which is higher than 0.70 V for **2**. With the purpose of explaining on a molecular basis the observed experimental differences, theoretical calculations for the electrogenerated intermediates were performed.

2.2. Employment of Fukui Functions and LUMO Densities for Describing Electron Acceptance Sites. In order to analyze the formation of the experimentally detected intermediates, analysis of the Fukui function was performed. As commented above, in an electron transfer process where the system gains electrons, the space dependent electron density, $\rho(r)$, and the spin density, $\rho_S(r)$, are also modified; thus, a description based on the Fukui function (eq 1)[25] requires consideration of both changes. Two general approaches have been proposed to deal with this situation: the frozen core and the finite differences approximations (FCA and FDA).[26] In terms of the spin-α and spin-β populations, $\rho(r)$ and $\rho_S(r)$ are defined as

$$\rho(r) = \rho_\alpha(r) + \rho_\beta(r) \quad (5a)$$

$$\rho_s(r) = \rho_\alpha(r) - \rho_\beta(r) \quad (5b)$$

In the case of a reduction process, where the electron uptake occurs from the original structure [Q]-ϕ-NO_2, the number of α electrons is increasing and the total electron density becomes[27]

$$\Delta\rho(r) \cong \left\{ \left(\frac{\partial \rho_\alpha(r)}{\partial N_\alpha} \right)_{N_\beta, v(r)} + \left(\frac{\partial \rho_\beta(r)}{\partial N_\alpha} \right)_{N_\beta, v(r)} \right\} \Delta N_\alpha \quad (6)$$

Employing the definition of the Fukui function, the terms in the right side of the equation are defined as

$$f^+_{\alpha\alpha}(r) = \left(\frac{\partial \rho_\alpha(r)}{\partial N_\alpha} \right)_{N_\beta, v(r)} \quad (7)$$

$$f^+_{\beta\alpha}(r) = \left(\frac{\partial \rho_\beta(r)}{\partial N_\alpha} \right)_{N_\beta, v(r)} \quad (8)$$

The positive sign indicates that the system is gaining electrons. In a closed-shell system, this process involves only

dx.doi.org/10.1021/jo500787q | J. Org. Chem. 2014, 79, 5201−5208

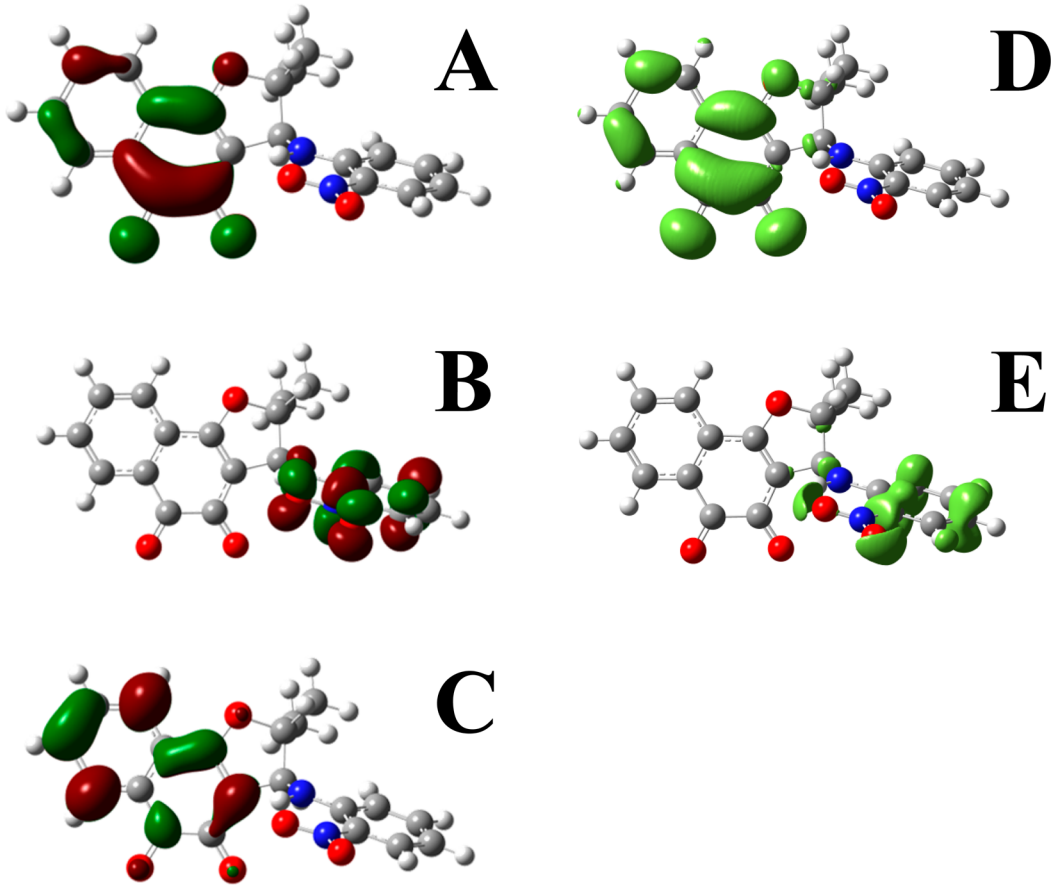

Figure 6. Isosurfaces obtained for **1**. (A–C) LUMO density for the neutral, radical anion and biradical dianion species, respectively, (D) $f^{+}_{\alpha\alpha}$ for the neutral species, (E) $f^{+}_{\beta\beta}$ for the radical anion species. Isosurfaces for LUMO densities are plotted as 0.04 Å^{-3}, while Fukui functions isosurfaces are plotted at 0.001 Å^{-3}.

changes in the electron population α orbitals and so the changes in spin-β density are not significant. Within the FDA approximation, the $f^{+}_{\alpha\alpha}$ Fukui function is defined by

$$f^{+}_{\alpha\alpha} \cong \rho^{\text{anion}}_{\alpha}(r) - \rho^{\text{neutral}}_{\alpha}(r) \tag{9}$$

In the FCA, the difference presented in eq 9 is approximately related to the density of the lowest α unoccupied molecular orbital (LUMO, α), and $f^{+}_{\alpha\alpha}$ can be calculated alternatively as

$$f^{+}_{\alpha\alpha} \cong |\varphi_{\text{LUMO},\alpha}(r)|^2 \tag{10}$$

Forthcoming reduction processes involve the uptake of electrons by an open-shell system ([Q$^{\bullet-}$]-ϕ-NO$_2$), leading to calculate, due to the expected differences between α and β densities, two additional Fukui functions:

$$f^{+}_{\beta\beta}(r) = \left(\frac{\partial \rho_{\beta}(r)}{\partial N_{\beta}}\right)_{N_{\alpha},v(r)} \tag{11}$$

$$f^{+}_{\alpha\beta}(r) = \left(\frac{\partial \rho_{\alpha}(r)}{\partial N_{\beta}}\right)_{N_{\alpha},v(r)} \tag{12}$$

The change in spin-β population is referred as the most significant in the description of the electron transfer process. Within the FDA, the corresponding Fukui function for analyzing the changes in spin-β population becomes

$$f^{+}_{\beta\beta}(r) \cong \rho^{\text{anion}}_{\beta}(r) - \rho^{\text{neutral}}_{\beta}(r) \tag{13}$$

In the FCA, this function is defined as

$$f^{+}_{\beta\beta} \cong |\varphi_{\text{LUMO},\beta}(r)|^2 \tag{14}$$

With these definitions, it is possible to analyze the spatial contributions of the corresponding Fukui functions (obtained by the FDA) for identifying the sites prone to electron acceptance and they can be compared with the LUMO density, which is the equivalent factor within the FCA. Figures 6 and 7 show plots of $f^{+}_{\alpha\alpha}$ of the neutral species, $f^{+}_{\beta\beta}$ for the radical anions, and the corresponding LUMO density isosurfaces for the studied compounds.

The isosurfaces obtained are in accord with the experimental results. For example, the first reduction process occurs in the quinone moiety, which presents the highest LUMO density and $f^{+}_{\alpha\alpha}$. Upcoming electron uptake takes place in the nitro function, since it presents the highest contribution to the LUMO density and also for $f^{+}_{\beta\beta}$. It should be noted that, even though it has been considered that the FCA approach cannot be considered as a general use approximation, the obtained results coincide for the analyzed molecules: LUMO densities are a fairly valid descriptors of the sites for electron uptake in the second redox group. Employing this approximation, the LUMO values for the corresponding biradical dianion is mainly located at the reduced quinone group, in agreement with the experimental results which indicate that the consumption of the quinone radical anion intermediate, at peak IIIc (Figures 3 and 5).

dx.doi.org/10.1021/jo500787q | J. Org. Chem. 2014, 79, 5201–5208

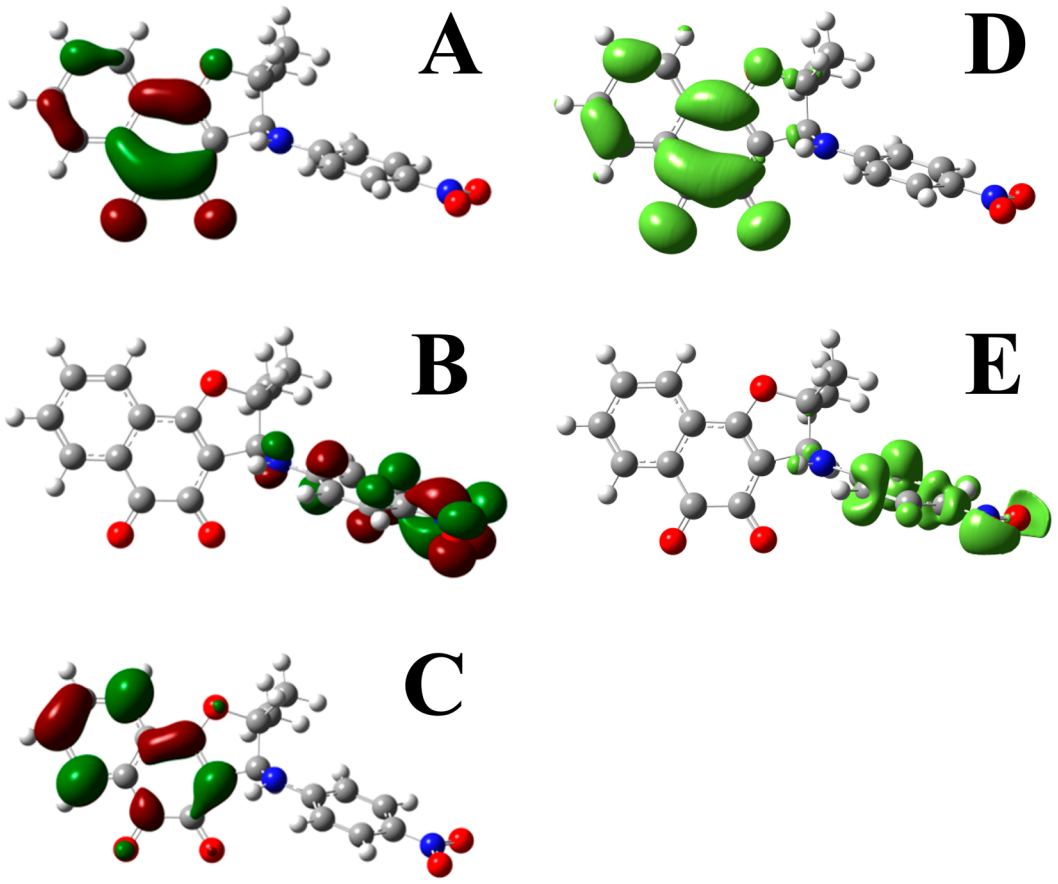

Figure 7. Isosurfaces obtained for **2**. (A–C) LUMO density for the neutral, radical anion and biradical dianion species respectively, (D) $f^{+}_{\alpha\alpha}$ for the neutral species, (E) $f^{+}_{\beta\beta}$ for the radical-anion species. Isosurfaces for LUMO densities are plotted as 0.04 $Å^{-3}$, while Fukui functions isosurfaces are plotted at 0.001 $Å^{-3}$.

Experimentally, it is noteworthy that the reduction of the corresponding semiquinone intermediate for the *ortho* compound (**1**) takes place at a less negative reduction potential than for the *para* isomer (**2**). This effect can be explained considering that for the *ortho* derivative, a possible interaction via ion-pairing between the semiquinone species and the corresponding cation of the supporting electrolyte takes place.[29] This interaction would be favored by the proximity between the negative charges at both redox centers, which are not close in the *para* compound (see the Supporting Information). Also, Sasaki and colleagues have commented that solvent effects strongly determine the potential value for the reduction of semiquinone species.[30]

The above presented results can be used for understanding the differences in biological activities referred in Table 1: The higher selectivity indexes observed for compounds **1** and **2** suggest that the formation of stable radical dianions is a prerequisite for increasing these values (Table 1). In the case of trypanocidal activities, the *ortho* compound **1**, which is significantly active (when compared with benznidazole), presents a less stable semiquinone intermediate, reduced at less negative potential values than the corresponding intermediate for the *para* compound (in turn less active): −1.73 for *ortho* vs −1.90 for *para*, Table 2. Further analysis employing condensed values of the Fukui functions will be used for other nor-β-lapachone and nor-α-lapachone derivatives.

3. CONCLUSIONS

In this work, electrochemical, spectroelectrochemical, and theoretical analyses of the reduction process in nor-β-lapachones derivatives including a nitro redox center are presented. In general, the reduction of the compounds involves, in the first step, the formation of a quinone radical anion, followed by the formation of a biradical dianion structure where both unpaired electrons are located on the quinone nucleus and the nitro group. The third reduction process is associated with the consumption of the first electrogenerated radical anion of the quinone forming the corresponding dianion. Theoretical descriptions of the corresponding Fukui functions $f^{+}_{\alpha\alpha}$ and $f^{+}_{\beta\beta}$(r) and LUMO densities considering both a finite differences and frozen core approximations for describing the changes in electron and spin densities of the system allowed the confirmation of these results. A description of the potential relationship of the results with the experimental selectivity indexes and trypanocidal activities suggest that in the former case, anticancer activities are related to the formation of stable dianion biradical species, whereas in the latter, stability of the semiquinone intermediates might be the determining factor.

4. EXPERIMENTAL AND THEORETICAL SECTION

4.1. Chemicals. Electrochemical studies were carried out using solutions of 2,2-dimethyl-3-(2-nitrophenylamino)-2,3-dihydronaphtho[1,2-*b*]furan-4,5-dione (**1**) and 2,2-dimethyl-3-(4-nitrophenylamino)-2,3-dihydronaphtho[1,2-*b*]furan-4,5-dione (**2**), which were synthesized according to a procedure described earlier.[31] Acetonitrile (CH_3CN) distilled from P_2O_5 and kept under molecular sieves was

dx.doi.org/10.1021/jo500787q | J. Org. Chem. 2014, 79, 5201–5208

used as solvent and tetrabutylammonium hexafluorophosphate (*n*-Bu_4NPF_6), recrystallized from hexane:ethyl acetate mixtures, dried the night before use at 105 °C, was used as supporting electrolyte. Solutions were maintained under an inert atmosphere by saturation with high-purity nitrogen at room temperature (approximately 20 °C) for 25 min before each series of experiments.

4.2. Instrumentation. Cyclic voltammetry experiments were performed using a potentiostat interfaced with a personal computer, applying IR drop compensation with Ru values determined from positive feedback measurements.[32,33] A glassy carbon disk electrode (0.07 cm^2), polished with 0.05 μm diamond powder (Buehler), and rinsed with acetone before each voltammetric run, was used as the working electrode. A commercial saturated calomel electrode (SCE), separated from the medium with a salt bridge filled with the supporting electrolyte solution and a platinum wire, were used as the reference and auxiliary electrodes, respectively. The potential values obtained are referred to the ferrocene/ferricinium (Fc/Fc^+) couple as recommended by IUPAC.[34] The potential for this redox couple, determined from voltammetric studies, was 0.41 V vs SCE.

ESR spectra was recorded in the X band (9.85 GHz), using a Bruker ELEXSYS 500 instrument with a rectangular TE102 cavity. A commercially available spectroelectrochemical cell was used. A platinum mesh (~0.2 cm^2) was introduced in the flat path of the cell and used as working electrode. Another platinum wire was used as counter electrode (2.5 cm^2). Ag/0.01 mol L^{-1} $AgNO_3$ + 0.1 mol L^{-1} tetrabutylammonium perchlorate reference in acetonitrile was employed as the reference electrode. Potential for the ferrocene/ferricinium couple vs this reference electrode was 0.38 V. Potential control was performed with a potentiostat to ensure the formation of each electrogenerated intermediate. The employed solutions were prepared with the same procedure as the ones used for the electrochemical studies. PEST WinSim free software Version 0.96 (National Institute of Environmental Health Sciences) was used to determine hyperfine coupling constant values (HFCC), in order to fit the experimental ones. This program was also used to evaluate HFCC values in the case when a direct measurement would be difficult under the spectra acquisition conditions.

4.3. Electronic Structure Calculations. Geometry optimization and frequency calculations of the neutral, radical anion and biradical dianion structures of **1** and **2** were carried out with the program Gaussian 09 Revision B.01,[35] using the approach of the density functional theory. The BHandHLYP[36] functional was employed as defined with a 6-311++G(d,p) basis set. Frequency analyses for all the involved structures were performed after full geometry optimizations, revealing the absence of negative frequencies, thus indicating that the structures are minimum energy conformers. Optimized structures were obtained, including the solvent effect by the Marenich, Cramer, and Truhlar model.[37] Single-point calculations were also performed on the optimized structures to determine the Fukui indexes for the neutral and radical anion structures.

■ ASSOCIATED CONTENT

Supporting Information

Internal coordinates as *Z*-matrices and calculated harmonic frequencies obtained for the minimum energy conformers for the neutral, anion radical, and biradical dianion structures for both structures. This material is available free of charge via the Internet at http://pubs.acs.org.

■ AUTHOR INFORMATION

Corresponding Authors

*E-mail: mofg@qui.ufal.br, mariliaofg@gmail.com.
*E-mail: ultrabuho@yahoo.com.mx, cfrontana@cideteq mx.

Notes

The authors declare no competing financial interest.

■ ACKNOWLEDGMENTS

G.A.V. thanks CONACyT-Mexico for support for his Ph.D. studies. C.F. thanks CONACyT-Mexico for support through Project 107037 "Convocatoria SEP-Conacyt Investigación Científica Básica, 2008). CNPq, CAPES, FAPEAL, and FAPEMIG (Brazil) are acknowledged for financial support.

■ REFERENCES

(1) Evans, D. H. *Chem. Rev.* **2008**, *108*, 2113.
(2) Astruc, D.; Boisselier, E.; Ornelas, C. *Chem. Rev.* **2010**, *110*, 1857.
(3) Flanagan, J. B.; Margel, S.; Bard, A. J.; Anson, F. C. *J. Am. Chem. Soc.* **1978**, *100*, 4248.
(4) Nepomnyashchii, A. B.; Bard, A. J. *Acc. Chem. Res.* **2012**, *45*, 1844.
(5) Nepomnyashchii, A. B.; Bröring, M.; Ahrens, J.; Bard, A. J. *J. Am. Chem. Soc.* **2011**, *133*, 8633.
(6) Saji, T.; Pasch, N. F.; Webber, S. E.; Bard, A. J. *J. Phys. Chem.* **1978**, *82*, 1101.
(7) Qi, H.; Chang, J.; Abdelwahed, S. H.; Thakur, K.; Rathore, R.; Bard, A. J. *J. Am. Chem. Soc.* **2012**, *134*, 16265.
(8) Meacham, A. P.; Druce, K. L.; Bell, Z. R.; Ward, M. D.; Kesiter, J. B.; Lever, A. B. P. *Inorg. Chem.* **2003**, *42*, 7887.
(9) Telo, J. P.; Moneo, A.; Carvalho, M. F. N. N.; Nelsen, S. F. *J. Phys. Chem. A* **2011**, *115*, 10738.
(10) Khajehpour, M.; Welch, C. M.; Kleiner, K. A.; Kauffman, J. F. *J. Phys. Chem. A* **2001**, *105*, 5372.
(11) de Abreu, F. C.; Ferraz, P. A. M.; Goulart, M. O. F. *J. Braz. Chem. Soc.* **2002**, *13*, 19.
(12) Squella, J. A.; Bollo, S.; Núñez-Vergara, L. J. *Curr. Org. Chem.* **2005**, *9*, 565.
(13) Hillard, E. A.; de Abreu, F. C.; Ferreira, D. C. M.; Jaouen, G.; Goulart, M. O. F.; Amatore, C. *Chem. Commun.* **2008**, 2612.
(14) Gilardi, G.; Fantuzzi, A. *Trends Biotechnol.* **2001**, *19*, 468.
(15) Araújo, A. J.; de Souza, A. A.; da Silva, E. N., Jr.; Marinho-Filho, J. B. D.; de Moura, M. A. B. F.; Rocha, D. D.; Vasconcellos, M. C.; Costa, C. O.; Pessoa, C.; de Moraes, M. O.; Ferreira, V. F.; de Abreu, F. C.; Pinto, A. V.; Montenegro, R. C.; Costa-Lotufo, L. V.; Goulart, M. O. F. *Toxicol. In Vitro* **2012**, *26*, 585.
(16) da Silva, E. N., Jr.; Guimaraes, T. T.; Menna-Barreto, R. F. S.; Pinto, M. C. F. R.; Simone, C. A.; Pessoa, C.; Cavalcanti, B. C.; Sabino, J. R.; Andrade, C. K. Z.; Goulart, M. O. F.; Castro, S. L.; Pinto, A. V. *Bioorg. Med. Chem.* **2010**, *18*, 3224.
(17) da Silva, E. N., Jr.; Souza, M. C. B. V.; Fernandes, M. C.; Menna-Barreto, R. F. S.; Pinto, M. C. F. R.; Lopes, F. A.; Simone, C. A.; Andrade, C. K. Z.; Pinto, A. V.; Ferreira, V. F.; Castro, S. L. *Bioorg. Med. Chem.* **2008**, *16*, 5030.
(18) da Silva, E. N., Jr.; de Deus, C. F.; Cavalcanti, B. C.; Pessoa, C.; Costa-Lotufo, L. V.; Montenegro, R. C.; de Moraes, M. O.; Pinto, M. C. F. R.; de Simone, C. A.; Ferreira, V. F.; Goulart, M. O. F.; Andrade, C. K. Z.; Pinto, A. V. *J. Med. Chem.* **2010**, *53*, 504.
(19) Hernández, D. M.; de Moura, M. A. B. F.; Valencia, D. P.; González, F. J.; González, I.; de Abreu, F. C.; da Silva, E. N., Jr.; Ferreira, V. F.; Pinto, A. V.; Goulart, M. O. F.; Frontana, C. *Org. Biomol. Chem.* **2008**, *6*, 3414.
(20) Parr, R. G.; Yang, W. *Density Functional Theory of Atoms and Molecules*; Oxford University Press: New York, 1989.
(21) Geerlings, P.; de Proft, F.; Langenaeker, W. *Chem. Rev.* **2003**, *103*, 1793.
(22) Sen, K. D.; Jorgensen, C. K.*Electronegativity, Structure and Bonding*; Springer: Berlin, 1987.
(23) Sen, K. D.*Hardness, Structure and Bonding*; Springer: Berlin, 1987.
(24) Pearson, R. G. *Chemical Hardness*; Wiley-VCH: New York, 1997.
(25) Parr, R. G.; Yang, W. T. *J. Am. Chem. Soc.* **1984**, *106*, 4049.
(26) Garza, J.; Vargas, R.; Cedillo, A.; Galván, M.; Chattaraj, P. K. *Theor. Chem. Acc.* **2006**, *115*, 257.

(27) Simón-Manso, E.; Valderrama, M.; Arancibia, V.; Simón-Manso, Y. *Inorg. Chem.* **2000**, *39*, 1650.
(28) Burkhardt, S. E.; Bois, J.; Tarascon, J. M.; Hennig, R. G.; Abruña, H. D. *Chem. Mater.* **2013**, *25*, 132.
(29) Macías-Ruvalcaba, N. A.; Evans, D. H. *J. Phys. Chem. B* **2005**, *109*, 14642.
(30) Sasaki, K.; Kashimura, T.; Ohura, M.; Ohsaki, Y.; Ohta, N. *J. Electrochem. Soc.* **1990**, *137*, 2437.
(31) Silva, R. S. F.; Costa, E. M.; Trindade, U. L. T.; Teixeira, D. V.; Pinto, M. C. F. R.; Santos, G. L.; Malta, V. R. S.; de Simone, C. A.; Pinto, A. V.; de Castro, S. L. *Eur. J. Med. Chem.* **2006**, *41*, 526.
(32) Roe, D. K.Overcoming Solution Resistance with Stability and Grace in Potentiostatic Circuits. In *Laboratory Techniques in Electroanalytical Chemistry*; Kissinger, P. T., Heineman, W. R., Eds.; Marcel Dekker: New York, 1996.
(33) He, P.; Faulkner, L. R. *Anal. Chem.* **1986**, *58*, 517.
(34) Gritzner, G.; Küta, J. *Pure Appl. Chem.* **1984**, *56*, 461.
(35) Gaussian 09, Revision B.01, Gaussian: Frisch, M. J.; Trucks, G. W.; Schlegel, H. B.; Scuseria, G. E.; Robb, M. A.; Cheeseman, J. R.; Scalmani, G.; Barone, V.; Mennucci, B.; Petersson, G. A.; Nakatsuji, H.; Caricato, M.; Li, X.; Hratchian, H. P.; Izmaylov, A. F.; Bloino, J.; Zheng, G.; Sonnenberg, J. L.; Hada, M.; Ehara, M.; Toyota, K.; Fukuda, R.; Hasegawa, J.; Ishida, M.; Nakajima, T.; Honda, Y.; Kitao, O.; Nakai, H.; Vreven, T.; Montgomery, J. A., Jr.; Peralta, J. E.; Ogliaro, F.; Bearpark, M.; Heyd, J. J.; Brothers, E.; Kudin, K. N.; Staroverov, V. N.; Keith, T.; Kobayashi, R.; Normand, J.; Raghavachari, K.; Rendell, A.; Burant, J. C.; Iyengar, S. S.; Tomasi, J.; Cossi, M.; Rega, N.; Millam, J. M.; Klene, M.; Knox, J. E.; Cross, J. B.; Bakken, V.; Adamo, C.; Jaramillo, J.; Gomperts, R.; Stratmann, R. E.; Yazyev, O.; Austin, A. J.; Cammi, R.; Pomelli, C.; Ochterski, J. W.; Martin, R. L.; Morokuma, K.; Zakrzewski, V. G.; Voth, G. A.; Salvador, P.; Dannenberg, J. J.; Dapprich, S.; Daniels, A. D.; Farkas, O.; Foresman, J. B.; Ortiz, J. V.; Cioslowski, J.; Fox, D. J. Gaussian, Inc., Wallingford, CT, 2010.
(36) Frisch, A.; Frisch, M. J.; Clemente, F. R.; Trucks, G. W.et al.*Gaussian 09 User's Reference*; Gaussian, Inc.: Wallingford, CT, 2009.
(37) Marenich, A. V.; Cramer, C. J.; Truhlar, D. G. *J. Phys. Chem. B* **2009**, *113*, 6378.